






<https://doi.org/10.1038/s43247-023-01029-4>

OPEN

Streamflow decreases in response to acid deposition in a subtropical forest watershed in China

Linhua Wang ¹, Matthew Lanning ², Lixin Wang ³, Mengxiao Yu¹, Shu Ye ¹, Lei Tian⁴, Haw Yen⁵ & Junhua Yan ¹✉

Streamflow reductions have been attributed to the impacts of soil nutrient availability on plant transpiration, connecting soil biogeochemical and hydrological processes. Here we conducted a plot-scale acid addition experiment and monitored long-term hydrology in a subtropical watershed to provide direct evidence for the underlying mechanisms of these connections. These results showed that acid deposition enhanced plant growth and thus increased plant transpiration in the early treatment period. It indicates that plants can increase their transport of water and nutrients to satisfy physiological demands under continuous acid deposition. Acid deposition mainly contributed to increased evapotranspiration and decreased streamflow at the watershed scale. These results provide complementary evidence of plants adjusting to acid deposition-induced changes in soil nutrient availability and these acclimations result in streamflow reductions at the watershed scale. Our results call for integrating forest biogeochemical feedback into watershed hydrology.

¹Key Laboratory of Vegetation Restoration and Management of Degraded Ecosystems, South China Botanical Garden, Chinese Academy of Sciences, Guangzhou 510650, China. ²Department of Geology and Environmental Sciences, The State University of New York at Fredonia, Fredonia, NY 14063, USA. ³Department of Earth Sciences, Indiana University Indianapolis, Indianapolis, IN 46202, USA. ⁴Institute of Green Development of the Yellow River Drainage Basin, Lanzhou University, Lanzhou 730000, China. ⁵School of Forestry & Wildlife Science, Auburn University, Auburn, AL 36849, USA. ✉email: jhyan@scib.ac.cn

Widespread atmospheric deposition of strong acid anions of sulfur (S) and nitrogen (N) aerosolized by anthropogenic processes is an important driver of plant nutritional status and uptake of forest soils and is inherently linked to plant growth and transpiration^{1–3}. For example, acid deposition can have a fertilization effect on plant growth by increasing the soil N availability or base cation mobilization^{4,5}. In addition, acid deposition can cause soil acidification and the leaching of base cations, such as calcium (Ca), magnesium (Mg) and potassium (K), thus reducing the availability of these nutrients for plants⁶. Moreover, acid deposition may aggravate the release of metal ions into the soil and soil solution in the form of hydrated oxides, particularly aluminum (Al)⁷. The increased mobilization of Al in the soil may inhibit root cell division and elongation^{8,9} and damage the root membrane structure and function, leading to blocked Ca uptake^{10–12}. Consequently, long-term acid deposition may impair plant growth because it leads to nutrient imbalances and hinders the nutrient uptake process. The resultant positive or negative effects associated with acid deposition are largely determined by the biogeochemical functions of the affected nutrients. However, the integrated physiological responses of plants to soil nutrient availabilities with regard to hydrological changes remain elusive, particularly in regions suffering from long-term acid deposition in subtropical or tropical forest ecosystems.

The hydrological cycle of forested watersheds involves three main fluxes: precipitation (P), evapotranspiration (ET), and streamflow (Q)¹³. Plant transpiration supports the continuous upward movement of water and nutrients from the soil to the vegetation^{14,15}, a crucial component linking soil biogeochemical processes and forest hydrology. Notably, soil calcium plays a crucial role in modulating plant physiological responses, such as stomatal closure regulation, carbohydrate metabolism and cell division¹⁶. Nutrient imbalances may drive plants to acquire nutrients for physiological demands through soil uptake and transpiration¹⁷. Thus, plant transpiration may be particularly sensitive to soil nutritional conditions^{18,19}. A study from the Hubbard Brook Experimental Forest (HBEF; New Hampshire) observed a short-term (3-year) increase in plant transpiration following soil Ca restoration because the increased Ca availability enhanced the primary production of trees²⁰. Another study from the Fernow Experimental Forest (FEF; West Virginia) reported that acid deposition could intensify plant water transport when plants underwent soil Ca deficiencies as observed in a long-term (30-year) acidified watershed²¹. Additionally, the elevated plant transpiration and reduced water drainage loss resulted from additional N being added into a field plot in an N-rich subtropical forest at the Dinghushan Biosphere Reserve (DBR, Guangdong Province)²². These results highlighted the soil biogeochemical effects on plant physiological processes, ultimately altering watershed hydrology. However, the abovementioned studies did not examine the stomatal or xylem hydraulic response to acid deposition, and Smith and Shortle²³ also pointed out the need for a microscale understanding of xylem hydraulic traits within a living tree. Tree leaf stomatal and xylem hydraulic traits may reflect the morphological and physiological adjustments of trees to changing environmental conditions, thus providing important information about water transport when coping with nutrient availability alterations resulting from acid deposition. Thus, the lack of direct evidence from leaf stomatal and stem xylem hydraulic structures at the individual tree level significantly constrains our understanding of the physiological mechanism behind the hydrological responses of forested watersheds to acid deposition.

Acid deposition affects soil biogeochemical processes and causes subsequent cascading changes in plant physiological

processes and hydrological dynamics. However, acid deposition does not affect plant transpiration in isolation; concurrent changes in P, air temperature, vapor pressure deficit (VPD), and elevated atmospheric carbon dioxide (CO₂) can also affect plant transpiration^{24–28}. For example, mounting studies have suggested that CO₂ has far-reaching impacts on ET through modified plant physiological processes²⁹. On the one hand, CO₂ may reduce stomatal conductance and diminish ET, thus increasing Q³⁰. On the other hand, this effect may be neutralized through the promotion of plant leaf growth, thus increasing the surface area on which transpiration occurs³¹. In addition, plant transpiration largely depends on stomatal apertures, which are profoundly regulated by VPD and air temperature^{32,33}. VPD reflects the atmospheric evaporative demand and connects ecosystem water cycles by regulating plant transpiration^{34,35}. These interactions that affect plant transpiration and streamflow highlight the need for additional observational datasets to separate the effects of acid deposition on plant physiological performance and hydrological processes. Acid deposition exerts previously unrecognized impacts on the hydrological cycle, the contribution of acid deposition to hydrological processes from the forested watershed perspective remains uncertain.

The primary objective of this study is to examine how the responses of plant physiological traits to acid deposition at the microscale connect with hydrological processes at the watershed scale. To fill this knowledge gap, we uniquely combine data from a controlled plot experiment, forest and soil inventory data, and watershed hydrology monitoring data. First, we initiated a long-term plot-scale experiment in 2009 to investigate leaf stomata, stem radial growth and xylem hydraulic conductivity through dendrochronological techniques in the DBR watershed. We addressed how the physiological traits of trees adjust to acid addition. We also used foliar stoichiometry to examine the potential base cation deficiency corresponding to acid input, particularly for the Ca-regulated stomatal closure process. Second, we established a permanent plot (1 ha) to monitor the soil geochemical properties and forest species composition under ambient acid deposition. From these data, we assessed changes in the base cation content corresponding to the plant nutrient availability in the forest soil. Combining the observed results of the physiological responses of trees to acid deposition, we used forest inventory data to extend the data from the individual tree level to the watershed scale. Third, we measured the hydrological cycle in the DBR watershed and applied the Budyko framework, a widely used tool coupled water supply (annual P) and energy availability (potential evapotranspiration) balance, to examine the relative importance of hydrological drivers. From this analysis, we quantitatively attributed the dynamics of ET and Q in the watershed with regard to acid deposition, climate factors and atmospheric CO₂ through an attribution analysis. Therefore, our findings of the physiological responses of trees to acid deposition experiments at the microscale and the hydrological processes at the watershed scale enabled us to improve the mechanistic understanding of how long-term acid deposition influences the watershed hydrological cycle.

Results

Tree stem xylem and leaf traits in response to acid deposition.

Tree growth and xylem hydraulic trait responses to experimental acid addition were observed directly from tree stem anatomy in this work. Tree rings were collected from *Castanopsis chinenses*, which is the most abundant tree species in the study area and makes up 44% to 59% of the total stand basal area derived from forest inventory data during 1999–2015. The tree ring widths (RW) during 2000–2008 showed very similar values prior to the

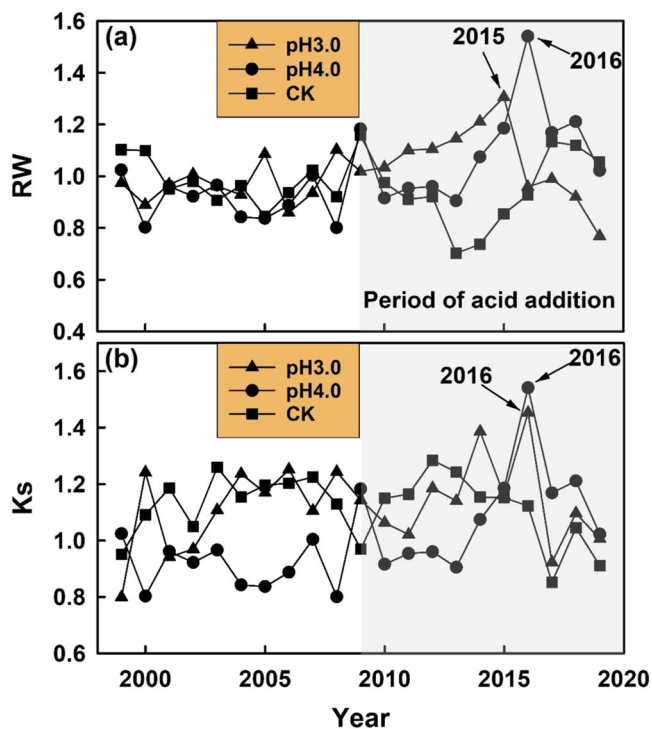


Fig. 1 The responses of tree growth and xylem hydraulic traits to experimental acid addition. **a, b** The tree-ring widths (RW) and theoretical xylem-hydraulic conductivity (Ks) within annual ring of *Castanopsis chinensis* in the treatment (pH3.0, pH4.0) and control plot (CK). The gray shaded areas indicate the period of experimental acid addition. The lines indicate the mean values measured from 6, 8 and 8 tree cores sampled from pH3.0, pH4.0 and CK, respectively.

treatment period (Fig. 1a). The RWs of trees growing in the treated plots gradually became larger than those in the control plots since the start of the acid addition in 2009 (Fig. 1a). The maximum RW deviation between the treated and control plots was observed after a 6–7 year period. Then, the RWs declined rapidly, and a similar stem radial growth was maintained during 2017 and 2019. Altered stem radial growth under acid addition could subsequently impact the xylem hydraulic traits; thus, acid addition might affect the xylem hydraulic conductivity (Ks) and mean vessel diameter (Dh) of annual rings. The Ks trend was consistent with the RW values after acid addition. Generally, the Ks and Dh of trees growing in the control plots remained relatively stable during the study period (Fig. 1b). For the treated plots, the Ks showed an obvious increasing trend during the first 6–7 years after acid addition (2009–2016) followed by steep decreases during 2017 and 2019. The Dh growing in the pH3.0 plots showed a slightly increasing trend, whereas a slightly decreased in Dh was observed in the pH4.0 plots during the whole experimental period (Supplementary Fig. 1). Overall, acid deposition has a short-term (6–7 years) fertilization effect on tree physiological processes, and the stem radial growth-enhancing effect ceases as indicated by the tree RW and Ks values with continuous acid application.

For tree leaf traits, the leaf stomatal densities of trees growing in the acid addition plots were consistently higher than those of trees growing in the CK plots, while the stomatal densities of *Aidia canthioides* Masam growing in the pH4.0 was slightly lower than in the CK (Table 1). The stomatal guard cell lengths in the acid addition plots were slightly larger (though not statistically significant) than those in the control plots. In addition, the foliar Ca contents in the acidified plots were significantly lower than

those in the control plot (Table 1). These reduced foliar Ca contents were an expected result of the loss of soil base cations induced by acid deposition. This foliar cation content is in line with previous observations of other tree species from plot-scale control experiments performed at the same site²². In addition, *Castanopsis chinensis*, *Schima superba* and *Pinus massoniana* (the tree species tested for their foliar Ca contents) were the dominant tree species in the study area, and the basal area of these three species increased from 94 to 96% between 1999 and 2015 (Fig. 2a). Similar foliar Ca content decreased with acid treatment for all tested tree species suggesting that the decrease is a generalized tree response to acid deposition. In addition, the iWUE of *Castanopsis chinensis*, a dominant tree species accounted for 44% to 59% of the total stand basal area, was 16% lower in the pH 3.0 plots compared to the control plots (Supplementary Fig. 2). Overall, acid addition showed no significant differences in iWUE of trees growing at treatment and control plots.

Soil base cation availability changed with acid deposition. The N and S deposition rates ranged from 25.1 to 53.4 and 37.7 to 72.5 kg ha⁻¹ yr⁻¹, respectively, and the rainwater pH generally varied from 4.5 to 5.6 from 2000 to 2018 (Supplementary Fig. 3). Although the acid deposition decreased by approximately 17% for N and 19% for S, the forested watershed still received large amounts of N and S, which continued to influence the soil properties. In general, the soil pH_{water} decreased from 4.1 to 3.8 ($S = -37$) under ambient acid deposition over the study period (Fig. 2b). Consistent with soil acidification, the leaching of soil Exch. Ca into the subsurface layer or Q losses (Supplementary Fig. 4) from the watershed would reduce the soil Ca content and stocks (Supplementary Fig. 5). The soil Exch. Al substantially increased and accounted for approximately 30.1 to 84.4% of the extractable cation pools (Fig. 2c). Therefore, long-term ambient acid deposition could promote soil acidification, the leaching loss of soil Ca, and the release of Al into the soil, which in turn may induce nutrient imbalances and cause nutrient deficiencies in vegetation.

Dynamics of Q and ET in the DBR watershed. The dynamics of annual P and Q in the DBR watershed were monitored over the period from 2000 to 2018. Overall, P exhibited a significant increasing trend ranging from 1278.6 to 2869.2 mm ($S = 56$) (Supplementary Fig. 6), while Q ranged from 368.5 to 1322.2 mm with a significant decreasing trend ($S = -52$) over the study period (Fig. 3a). The soil water storage of 0–50 cm was relatively stable and the annual difference was less variable with ranged from –26.1 to 20.2 mm (Supplementary Fig. 6). The annual ET derived from the water-balance method exhibited a significant increasing trend ($S = 114$) (Fig. 3b). This significant positive trend arose from the increasing trend in P, coupled with a decreasing trend in Q from 2000 to 2018. The ratio of ET and P (ET/P) indicates the fraction of P returned to the atmosphere. We found that ET/P varied from 22 to 72% and exhibited an increasing trend, whereas the annual runoff coefficient declined during the past two decades (Fig. 3a, b). These results indicated that despite the increase in P, the ET increase outpaced the P increase during the study period, resulting in a decreased Q.

Potential evapotranspiration (PET) is a key component for understanding the watershed water balance in the Budyko framework, as shown in Fig. 3c. In this study, PET was derived from climate variables, including the air temperature (T), net radiation (Rn), relative humidity (Rh) and wind speed (U_2), and showed an increasing trend ($S = 27$) (Supplementary Fig. 7). In addition, Rh significantly increased ($S = 47$), while Rn ($S = 23$), U_2 ($S = 3$) and T ($S = 1$) showed slightly increasing trends during

Table 1 The responses of leaf traits to experimental acid addition.

Tree species	Treatment	Foliar Al Content (mg g ⁻¹)	Foliar Ca Content (mg g ⁻¹)	Stomatal Density (No. mm ⁻²)	Guard Cell Length (um)
<i>Castanopsis chinensis</i>	CK	0.75 ± 0.10 a	6.38 ± 0.69 a	269 ± 53 b	21.8 ± 0.9 a
	pH4.0	0.96 ± 0.29 a	4.01 ± 0.78 b	286 ± 89 b	22.9 ± 2.7 a
	pH3.0	0.59 ± 0.34 a	2.74 ± 0.25 b	320 ± 37 a	22.1 ± 0.7 a
<i>Aidia canthioides</i> Masam.	CK	0.35 ± 0.07 a	10.73 ± 3.02 a	298 ± 53 b	28.4 ± 2.7 ab
	pH4.0	0.40 ± 0.06 a	8.20 ± 2.06 b	279 ± 60 b	28.9 ± 2.8 a
	pH3.0	0.39 ± 0.08 a	7.63 ± 1.43 b	328 ± 79 a	28.9 ± 1.6 a
<i>Cryptocarya concinna</i> Hance	CK	0.29 ± 0.05 a	5.60 ± 1.19 a	76 ± 23 a	21.2 ± 1.9 ab
	pH4.0	0.28 ± 0.01 a	4.00 ± 0.04 b	79 ± 20 a	21.2 ± 0.8 ab
	pH3.0	0.32 ± 0.08 a	4.20 ± 0.37 ab	87 ± 26 a	22.1 ± 1.8 a
<i>Aporosa yunnanensis</i> Metc.	CK	30.81 ± 2.50 a	23.55 ± 2.05 a	298 ± 59 c	22.1 ± 1.0 a
	pH4.0	27.97 ± 5.75 a	19.40 ± 4.55 b	346 ± 53 ab	22.0 ± 1.2 a
	pH3.0	29.17 ± 2.50 a	18.85 ± 3.14 b	353 ± 66 a	22.2 ± 0.8 a

The leaf traits included foliar calcium (Ca), aluminum (Al) content and leaf stomatal density and its guard cell length for common tree species in the treatment (pH3.0, pH4.0) and control plot (CK). One-way ANOVA was used to assess whether there is a significant difference between different treatments for a tree species. The treatments are acid addition with solution at pH 4.0 (pH4.0) and 3.0 (pH3.0), and control plot (CK). The values indicate the mean ± standard deviation with three replicates. Different lower letters for a tree species denote significant differences ($p < 0.05$).

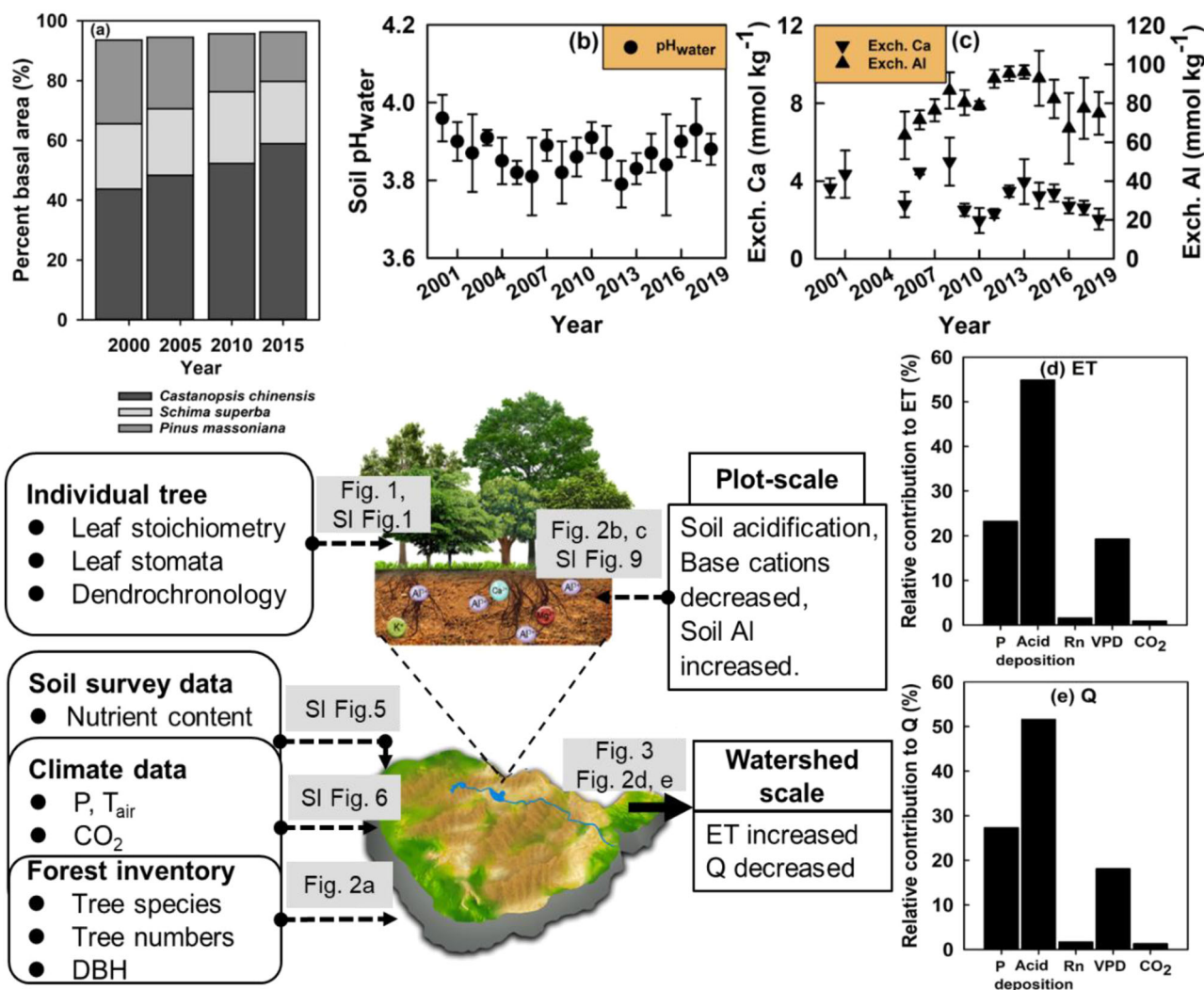


Fig. 2 A conceptual diagram showing how soil biogeochemical processes altered by acid deposition affect plant transpiration at tree level and plot-level as well as affect hydrological processes at watershed scale. **a** The forest inventory data at watershed scale. **b, c** Acid deposition driven soil acidification with decreased base cations and elevated aluminum content. **d, e** The roles of precipitation (P), acid deposition, net radiation (Rn), vapor pressure deficit (VPD) and atmospheric CO₂ in the dynamics of evapotranspiration (ET) and streamflow (Q) from the forest watershed. The error bars represent the standard deviation obtained from independent measurements. SI supplementary information.

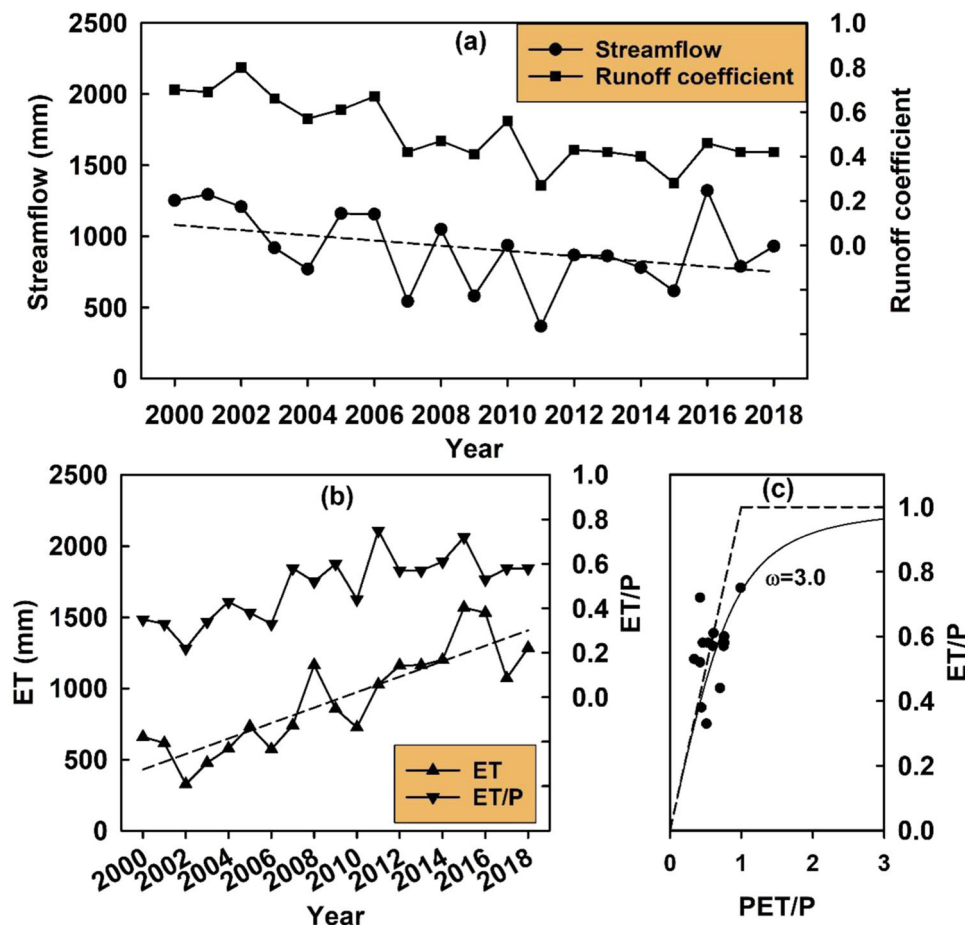


Fig. 3 Dynamics of observed streamflow (Q) and evapotranspiration (ET). **a** Dynamics of Q and the runoff coefficient, calculated as the ratio of Q to P, during 2000–2018. **b** Water balance-derived ET and ET/P, calculated as the ratio of ET to P, in the DBR watershed during 2000–2018. The dash line in **a** and **b** indicate average Q and ET trends during study period, respectively. **c** Scatterplot of potential evapotranspiration (PET)/P against ET/P and the solid line is the relationship represented by Fu's equation. The 1:1 dash line in **c** indicate that ET is limited by available energy, and the horizontal dash line in **c** indicate that ET is limited by available water for a watershed.

the study period. We applied a partial correlation analysis to evaluate the PET sensitivity to each climate variable. These results indicated that PET was attributable to Rn, which contributed approximately 60% of the PET increase (Supplementary Fig. 8). Thus, Rn was regarded as the main driver of the PET increase during the study period. In the Budyko framework, the hydrological components of ET and Q are shaped by the P (water supply), PET (energy supply) and watershed characteristics (ω). Combining the abovementioned changes in PET and P, the elasticities of ET to P, PET and ω were 0.68, 0.62 and 0.75, while the elasticities of Q to P, PET and ω were 0.87, -0.61 and -0.74 , respectively. This implies that ET and Q were most sensitive to ω and P, respectively. In addition, ω contributed 62.9% of the increased ET and 58.4% of the decreased Q during the study period. Our findings suggested that in addition to P and PET, watershed characteristics (ω), including the watershed topography, soil properties and vegetation dynamics, greatly contributed to the dynamics of ET and Q. Therefore, the potential impacts of ω on ET and Q become an important factor for investigating watershed hydrology.

In addition, the acid deposition amount could explain 72% of the ω variability (Supplementary Fig. 8). Given that acid deposition plays a fundamental role in soil nutrient and tree physiology processes, it is reasonable to examine the contribution of acid deposition to watershed hydrological processes. Therefore,

we evaluated the roles of P, acid deposition, Rn, VPD, and atmospheric CO_2 in the dynamics of ET and Q from the DBR watershed by conducting a partial correlation (R-value) analysis. We found that ET and Q were significantly and positively correlated with P (Fig. 4). An increased Rn is expected to increase ET ($R_{\text{ET-Rn}} = 0.079$), although not statistically significant, and thus reduce Q ($R_{\text{Q-Rn}} = -0.091$) in our watershed (Fig. 4a). The elevated CO_2 and VPD exhibited a negative correlation with ET and a positive correlation with Q, although these correlations were not statistically significant (Fig. 4b). Specifically, we found that ET was significantly and positively correlated with acid deposition ($R_{\text{ET-Acid deposition}} = 0.695$), while Q was significantly and negatively correlated with acid deposition ($R_{\text{Q-Acid deposition}} = -0.685$) (Fig. 4). Our results corroborate recent findings of an intensification of vegetation water use drawn from an acidification watershed experiment²¹. Additionally, we calculated the relative contribution of each factor to ET and Q to further reinforce the partial correlation analysis results. The results of the relative importance analysis showed that 54.9% and 51.6% of the ET and Q were attributable to acid deposition. The P contributed 23.3% and 27.3% of the observed variability in ET and Q, while VPD explained 19.3% and 18.1% of the observed variability in ET and Q, respectively (Fig. 2d, e). Therefore, these results suggested that acid deposition acts as an important contributor to the increased ET and decreased Q observed over the study period.

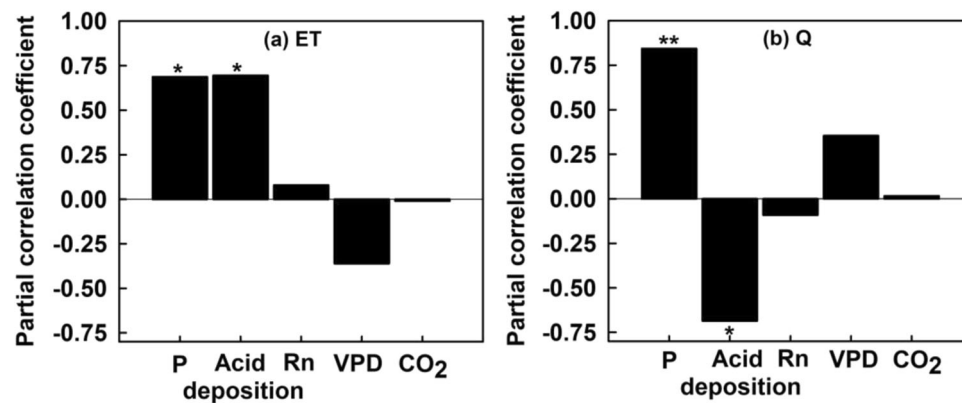


Fig. 4 The comparison of partial correlation coefficients between evapotranspiration (ET), streamflow (Q) and potential drivers. **a, b** Partial correlation coefficients between ET, Q and potential drivers, respectively. The black column indicates the partial correlation coefficient. The selected drivers are precipitation (P), net radiation (Rn), vapor pressure deficit (VPD), atmospheric CO₂ concentration (CO₂), and acid deposition. * and ** indicate that the significant partial correlation coefficients at $p < 0.05$ and $p < 0.01$, respectively.

Discussion

Within our field experimental design, data representing the leaf and xylem hydraulic traits of trees growing under simulated acid deposition allowed us to separate the effects of acid addition from other factors. Our evidence of the morphological and physiological traits of leaves and stems at the living tree level revealed that the trees experienced a short-term increase in stem radial growth with a greater xylem hydraulic conductivity to meet the large water use during the initial 6–7 years of treatment. For the initial short-term period, tree growth responded positively to the improved soil fertility due to the unparalleled level of nutrient availability released into the soil solution after acid addition in the N-rich subtropical forest. Our results were consistent with a temporary increase in ET due to the fertilizer effect of calcium addition at the HBEF²⁰. The direct restoration of a limiting nutrient in the HBEF case study²⁰ and the input N and increased base cation mobilization after acid addition in our field experiment essentially improved forest fertility in the early years of treatment, thus stimulating plant growth and boosting tree water use. Our results further provide physiological evidence of stem anatomical traits characterizing the increased plant transpiration response to the initial phase of acid addition.

However, this increased stem radial growth cannot be sustained, as indicated by the reduced RW under continuous acid addition compared with the RW at CK (Fig. 1). Similar patterns of initial increasing radial growth followed by decreasing growth under prolonged acid deposition have been found in other studies^{36–38}. In contrast to acid addition not significantly changing soil N concentration after 12-year, continuous acid input will eventually reach an excessive level and accelerate the base cation leaching loss, thus reducing the stocks and availability of base cations (Supplementary Fig. 9), which in line with the previous finding that the base cations depletion as a consequence of ongoing acid deposition³⁹. The observed decreased foliar Ca content suggested that plant Ca availability was consistently reduced under acid addition (Table 1). Given the signaling roles of Ca in regulating stomatal closure¹⁶ coincided with lowered soil Ca availability induced by continuous acid addition, trees with a higher leaf stomatal density may uptake more water to drive soil Ca flows to roots and satisfy Ca demand and thus induce a lower water use efficiency^{21,22}. Noteworthy is that litterfall (a proxy of plant primary productivity) showed no significant differences among acid addition and controlling plots (Supplementary Fig. 10). These results indicated that lowered base cations availability may drive plants to allocate more photosynthates to

belowground for growing roots and increase root exudations to mycorrhiza to improve uptake of soil water and nutrients, thus reducing photosynthates for stem radial growth. This interpretation is strongly supported by a recent work in tropical forests, suggesting who found that exchangeable base cation availability primarily drive plant to allocate more photosynthates to belowground that in turn reduce aboveground stem growth⁴⁰. Moreover, an acid addition study at the DBR site found that the plant allocates more photosynthates to mycorrhizal fungi to alleviate the acidification-induced soil phosphorous limitation in the same acid addition plots⁴¹. This result probably explained that no significant differences in litterfall among treated plots. Indeed, recent studies highlighted that soil nutrient availability plays a key but overlooked role in plant carbon allocation and growth. In line with the recent conceptual framework^{42,43}, our data on lowered soil base cation availability induced by long-term acid addition may drive plants to deliver more photosynthates to belowground to enhance nutrient availability, subsequently reducing photosynthates to stem radial growth (Fig. 1). Combining the decreasing soil Exch. Ca, shifts in the foliar Ca contents of dominant trees and forest inventory data, the increased plant transpiration adjusted to the nutrient imbalances induced by long-term acid deposition at the individual tree level can be scaled up to a higher vegetation community. These findings potentially have great implications in soil geochemistry effects on watershed hydrology through mediating plant physiological functions.

The watershed-scale ET, calculated by the water-balance method, exhibited an increasing trend; consequently, Q decreased from 2000 to 2018. The abovementioned results raise important questions about the contribution of acid deposition to regulating hydrological processes in a forested watershed. Our results showed that ET and Q are more sensitive to ω than P or PET in our watershed, as derived from the Budyko framework. In addition, the relative contributions of ω to the increased ET and decreased Q were approximately 62.9% and 58.4%, respectively; these values were higher than the relative contributions from P and PET. These results indicated that ω has become a dominant driver regulating ET and Q changes and represents the watershed topography, vegetation cover and soil properties. These results are in line with previous studies that found ω is the major cause of streamflow dynamics^{44,45}. At our study site, we assume that the topography and vegetation cover remain stable because this watershed is located within a biosphere reserve and has not been disturbed. Thus, we argue that the observed changes in ET and Q at the watershed scale result from tree transpiration adjusted to

altered soil geochemical properties induced by acid deposition. Indeed, our data suggested that the forest soils experienced a pronounced acidification process with reduced base cation contents and substantially increased soil Exch. Al over the study period (Fig. 2b, c, Supplementary Fig. 5). The reduced availability of soil Ca, its physiological importance in stomatal regulation, and its coincidence with the increased soil Al stimulated trees to take up more water and thus reduced the streamflow.

In addition, we applied a partial correlation analysis to investigate the responses of ET and Q to climate factors, CO₂ and acid deposition. The results indicated that the increased ET and decreased Q were dominantly attributable to P and acid deposition. However, the relative contribution of acid deposition was higher than the relative contribution of P to ET. Although the increased P had positive effects on Q, the negative effects of acid deposition on Q largely outweighed the positive effects of P, thus leading to an overall decrease in Q. In addition, our results indicated that the raised CO₂ had little impact on ET during the past two decades, in line with the previous findings that the low nutrient availability may explain these limited CO₂ effects⁴⁶. Indeed, our data on the decreasing soil Ca content support the notion that nutrient availability may play an important role in mediating the vegetation physiological response to the rise of CO₂. In particular, subtropical forest ecosystems are enriched with N, and increased plant transpiration is more likely in these areas due to acclimation to low base cations conditions driven by excessive acid input into deeply weathered soils. Our current results illustrated that soil calcium, a rock-derived nutrient, has profound effects on watershed hydrology through tree physiological processes and thus highlighted the importance of the calcium biogeochemical function in ecosystem processes in sub- or tropical forests. Indeed, the recent findings call attention to the impacts of calcium availability, apart from N and P, on tropical forest physiological and ecological processes⁴⁷. Given the assumption that the nutrient imbalance induced by acid deposition continues, the morphological and physiological adjustment responses of plants to nutrient availability may modulate plant transpiration and nutrient acquisition processes, and thereby regulate the hydrological cycle. In this context, a recent meta-analysis suggested that N deposition could increase leaf area and transpiration rate, thus lead to enhanced vegetation water requirement⁴⁸. Collectively, we built a conceptual framework, together with the recent findings^{21,22}, to illustrate how acid deposition alters soil biogeochemical properties linked to tree physiological acclimation at the tree level and further extends to hydrological processes at the watershed scale (Fig. 2). These results highlighted the critical role of vegetation physiological response to nutrient availability in watershed hydrology.

We found that the response of plant growth to acid deposition has a detectable impact on watershed discharges based on field manipulation experiments and watershed-scale observations. Our results thus improve the understanding of how acid deposition affects hydrological cycles through vegetation physiological responses. We do not mean to diminish the vital roles of climate conditions and land-use changes in determining hydrological processes^{32,49,50}. We also understand that our results have uncertainties. Since the DBR watershed is located in a biosphere reserve and vegetation cover is nearly complete, we used ET as a proxy for vegetation transpiration, not separating soil evaporation. We quantified and interpreted long-term changes in ET based on the water-balance method, which relied on field observations of P, Q and soil moisture storage through meteorological and hydrological measuring stations. The observed P data agreed well with P extracted from remote-sensing datasets, indicating that the field observation-based P is reliable in our study (Supplementary Fig. 11). Some uncertainties come from

variations in soil water and groundwater storage, which have been assumed to be negligible at an annual scale when calculating watershed ET. Particularly, recent studies emphasized that plants can access deep moisture stored in the soil or regolith layer regardless of the soil moisture content in the shallow layer^{51,52}. Thus, the storage of deep soil or rock moisture can be used to support plant transpiration and cannot be neglected, particularly in subtropical soil associated with highly weathered regolith and deep-rooted plants^{53,54}. The watershed hydrological dynamics coevolved with the climate, vegetation, soil, and regolith properties⁵⁵. To reduce the uncertainties in assessing the magnitude of these factors impact on water balance components, it is necessary to continue field manipulation experiments and observations on meteorological, hydrological and edaphic properties and other ancillary data, such as watershed architecture and groundwater depth. We also acknowledge that we only monitored the stem xylem anatomy and hydraulic traits of one dominant tree species (*Castanopsis chinenses*), a ring-porous species that exhibited an increase from 44% to 59% of the total basal area in our study watershed. During this inventory measurement period, *Schima superba*, a diffusive-porous species, retained 21 to 24% of the total basal area, whereas *Pinus massoniana*, a nonporous species, decreased from 28% to 17% in the total basal area. The response of tree growth to chronic acid deposition is regarded as species-specific and that diffusive-porous species exhibit reduced growth⁵⁶. If this species-specific response to acid deposition applies to our study site, in addition to our results, we need to examine more interspecific physiological adjustments to nutrient availabilities, particularly for decreasing base cations and N-rich subtropical forests. In addition, it should be noted that the enhanced K_s of trees result from an increased D_h during the period of plant adjustment to low levels of base cations caused by acid deposition (Supplementary Fig. 1). These results can be interpreted as an increased K_s increasing the risk of hydraulic failure, which could result in tree mortality. Ultimately, an increased K_s drives a shift in species composition and thus changes the watershed hydrology, indicating that a shift from ring-porous to diffusive-porous dominant species can lead to a long-term reduction in streamflow⁵⁷. These adaptive changes can increase the plant water use and transpiration processes, thus driving nutrients into plant tissues and consequently inducing changes in plant hydraulic structures to fulfill the water transportation demand. Regarding this aspect, our results further motivate the need to clarify how soil nutrient availability mediates tree growth, species succession and its interactions with climate change on forest hydrology in acid-impacted and N-rich forest ecosystems.

Overall, our results provided evidence to advance our mechanistic understanding of increased plant transpiration due to increased growth in the initial years and the reduced availability of base cations under prolonged acid deposition. Despite remaining uncertainties, we expect our results are robust to highlight how plants physiological traits adapt to deposition-driven changes in forest nutrients and provide insights into water cycling at forested watersheds in response to acid deposition. Such results explicitly reinforced that plant response to acid deposition plays a non-negligible factor in mediating hydrological cycle, and provided a biogeochemical understanding of forest watershed hydrology in addition to climate factors.

Methods

Study site. This study was conducted at the Dinghushan Biosphere Reserve (DBR) (23°10′–23°12′N, 112°31′–112°34′E), located in Zhaoqing city, Guangdong Province, China (Supplementary Fig. 12a). The DBR covers an area of 1155 ha and ranges

in elevation from 14 to 1000 m above sea level. This region has a typical subtropical monsoon climate. The annual mean minimum and maximum temperatures are 12.0 °C in January and 28.0 °C in July, respectively. The average annual P is approximately 1900 mm, of which approximately 80% occurs from April to September. The highly-weathered soils in this region are classified in the Ultisols order of the United States Department of Agriculture (USDA) soil taxonomy system and are derived from sandstone and shale parent material⁵⁸. The major tree species are *Castanopsis chinensis*, *Schima superba*, *Pinus massoniana*, *Cryptocarya chinensis*, *Aporosa yunnanensis*, *Blastus cochinchinensis*, *Ardisia quinquegona* and *Psychotria rubra*. The DBR joined the Chinese Ecosystem Research Network (CERN) initiated by the Chinese Academy of Sciences (CAS) in 1991 (<http://dhf.cern.ac.cn/content?id=40684>). The DBR was selected as the pilot station of the National Field Research Station network organized by the Ministry of Science and Technology of China in 1999. A meteorological station (M520, Vaisala, Finland), installed at a hilltop, is used to monitor the precipitation amount, air temperature, relative humidity etc. according to the mission of the Chinese Ecosystem Research Network (CERN) (Supplementary Fig. 12b). For validating the precision of monitoring precipitation dataset, monthly precipitation in DBR for 2000–2018 was also obtained from the China Meteorological Forcing Dataset (CMFD), Multi-Source Weighted-Ensemble Precipitation (MSWEP) and Climate Hazards group Infrared Precipitation with Stations (CHIRPS). The CMFD is based on remote sensing products, reanalysis datasets and in-situ station data and is specifically developed for studies of land surface processes in China. This dataset has a 3-hourly temporal resolution and 0.1° spatial resolution⁵⁹. The MSWEP is a recently released global precipitation dataset with a 3-hourly temporal resolution, covering the period 1979 to the near present^{60,61}. The dataset is based on the complementary strengths of gauge-, satellite-, and reanalysis-based data to produce global precipitation estimation. The CHIRPS is a new quasi-global (50°S–50°N) precipitation dataset with daily, pentadal and monthly precipitation at a spatial resolution of 0.05°, covering the period 1981 to the near present⁶².

Sampling and measurement in experimental acid addition plots.

The acid deposition simulation in the DBR watershed was initiated in June 2009. All treated plots had similar forest compositions and topography, and the differences among plots arose from different acid addition levels. These plots were surrounded by concrete panels inserted 15 cm into the topsoil layer to prevent surface runoff from flowing out of each plot. Two acid intensities were simulated with solution pH values of 4.0 (pH4.0) and 3.0 (pH3.0). Plots applied to local lake waters with a pH was about 4.5 and a low base cation concentration (Ca: 0.2–1.8 mg L⁻¹, Mg: 0.3–0.7 mg L⁻¹, K: 0.3–1.1 mg L⁻¹ during 2009–2020) were selected as the control group (CK). Further, the large quantity of lake water used each time is convenient to obtain in the actual field condition. Each treatment had three replicated plots and thus, nine plots (10 m × 10 m) were established. The simulated acidic solution was prepared by mixing H₂SO₄ and HNO₃ at a 1:1 mole ratio into the lake water. At each application time, 40 liters were applied to each plot at an interval of two weeks throughout the experimental period. Thus, the added H⁺ amount was 9.6 and 96.0 mol H⁺ ha⁻¹ year⁻¹ for the pH 4.0 and pH 3.0 treatments^{41,63}. Meanwhile, the added base cation amount was about 0.23, 0.19 and 0.13 mol H⁺ ha⁻¹ year⁻¹ for Ca, Mg, K, which was substantially lesser than acid input. The experimental acid solution was sprayed below the tree canopy using a gasoline engine sprayer. Litterfall was monthly collected during 2012, 2020 and 2021. A nylon litter trap (1.0 m × 1.0 m in size and 1.0 m

above the ground) with a mesh size of 1 mm was installed in each plot.

Tree foliage was collected in each treated plot in December 2020. Foliar samples were divided into two parts. One part was used for stomatal density and guard cell length measurements, and the other was oven-dried at 60 °C for subsequent nutrient content and carbon isotopes analysis. The measurement methods are described in the supplementary material (Supplementary Table 1). Due to the small plot area (10 m × 10 m), the main tree species in the experimental plots were *Castanopsis chinensis*, and this species was found to be the dominant species at our study site based on forest inventory data. Thus, two cores per tree with stem diameter >20 cm were collected at breast height using a 5-mm increment borer, and the total numbers of tree-ring samples taken were 6, 8 and 8 for pH 3.0, pH 4.0 and control plots, respectively. The procedure of the tree-ring cores processing follows standard dendrochronological techniques⁶⁴. Each core sample was glued on a wooden strip and air-dried. The cores were polished with progressively fine sandpaper at different grits (300/600/800/1200) to a clear and flat surface, and then chalk was added to the vessel lumina. Digital images of the polished cores were captured by a scanner (Epson TSD4800 flatbed scanner) at a 2400-dpi resolution. The tree-ring width (RW) was conducted using the ROXAS software from scanned images. The RW from two cores of the same tree was visually cross-dated and also statistically checked by *t*-test and Gleichläufigkeit values⁶⁵. Then, the quality of cross-dating was evaluated by the COFECHA program and then the cross-dated samples were detrended with the negative exponential model method using the Dendrochronology program library in R (dplR) conducted in R statistical software^{66,67}. Finally, all vessel parameters (e.g. vessel number, tangential and radial diameter, vessel area) were measured for each dated tree-ring and then calculated hydraulic conductivity (Ks) and mean vessel diameter (Dh) of annual rings in ROXAS software⁶⁸.

Sampling and measurement in the permanent plot. Southern China has suffered severe acid deposition within the past decades, and the DBR is an appropriate site for studying the effects of acid deposition on the processes and functions of subtropical forest ecosystems^{1,69–71}. Forest inventories were conducted in the 1.0-ha permanent plot in 1999, 2004, 2010 and 2015. Trees with diameters at breast height larger than 2.5 cm were included, and the trees were identified and counted by species name. Soil samples were also collected with four replicates from the 0–20 cm layer in the permanent plot. The soil samples were air-dried, one part was passed through 2-mm mesh, and the other part was passed through 0.25-mm mesh for further chemical measurements. The soil chemical properties, including the soil pH_{water}, cation exchange capacity (CEC), soil exchangeable potassium (Exch. K), calcium (Exch. Ca), magnesium (Exch. Mg) and aluminum (Exch. Al), were measured in the laboratory. Details of these measurements are provided in the supplementary material (Supplementary Table 1). Soil samples were collected to test soil moisture content (SMC) monthly using a 30-mm diameter hand-held auger at depths of 0–15, 15–30, and 30–45 cm in each permanent plot. The soil samples were oven-dried at 105 °C for 24 h. For each soil profile, soil samples were collected at intervals of 15 cm for soil bulk density measurements using a 100 cm³ soil corer. Thus, the soil water storage at certain depths was calculated based on the average monthly SMC and bulk density.

Watershed hydrology. The daily streamflow (Q) was automatically measured at the outlet of the DBR watershed (6.1 km²) since 2000 and used digital equipment (WGZ-1, Huazheng,

Chongqing, China) installed as a rectangular hydrological weir (Supplementary Fig. 12c)⁷². The staff of DBR resided in this field observatory station and regularly checked streamflow data and collected streamflow samples. Streamflow samples were manually collected at the hydrological weir in January, April, July and October during 2000–2018. Three streamflow samples were collected at each time and in total 228 samples were collected during the study period. The collected streamflow samples were filtered through 0.45 µm filters and stored in a cooler (4 °C). The concentrations of Ca (Stream. Ca), Mg (Stream. Mg) and K (Stream. K) in the streamflow were measured by a flame atomic adsorption spectrophotometer (GBC932AA, Australia), and the average values in stream water were used as the annual mean concentrations. In this study, we selected Fu's equation⁷³, one of the commonly used functional forms for estimating ET, and examined the dominant drivers of hydrological changes^{45,74}. The details of calculations were provided in the supplementary information.

Data analysis. The annual mean atmospheric CO₂ concentration (eCO₂) was derived from published datasets obtained from Mt. Waliguan station (35°17'N, 100°54'E), China, under the framework of the World Meteorological Organization/Global Atmosphere Watch^{75–78}. The water balance-derived annual ET was estimated by subtracting the observed annual Q and interannual soil water storage variations from the observed annual P at the watershed scale²⁰. The annual runoff coefficient was calculated as the ratio of annual Q to the annual P amount. Since acid deposition continuously impacts soil biogeochemical processes, we used cumulative acid deposition as a variable to characterize the effects of acid deposition on hydrological processes.

The nonparametric Mann-Kendall test was used to analyze trends and their significance over the study period. A positive “S” value indicates an increasing trend, while a negative “S” value indicates a trend that is decreasing over time^{21,79}. A partial correlation coefficient was also calculated to detect the statistical contribution of each factor after statistically excluding the effects of other factors^{80,81}. All analyses were conducted using Statistics Package for Social Science (SPSS) Version 2 with significance levels of $p < 0.05$ and $p < 0.01$. All the figures were created using SigmaPlot 14.0.

Data availability

All datasets used in this study can be accessed from the following link: <https://doi.org/10.6084/m9.figshare.23984694.v2>.

Received: 29 November 2022; Accepted: 28 September 2023;

Published online: 09 October 2023

References

- Lu, X., Mao, Q., Gilliam, F. S., Luo, Y. & Mo, J. Nitrogen deposition contributes to soil acidification in tropical ecosystems. *Glob. Chang. Biol.* **20**, 3790–3801 (2014).
- Ekstrom, S. M. et al. Effect of acid deposition on quantity and quality of dissolved organic matter in soil-water. *Environ. Sci. Technol.* **45**, 4733–4739 (2011).
- Qian, Q. et al. Assessment of acid deposition effects on water quality of the upper Rio Grande River section in Texas. *J. Water Resour. Prot.* **05**, 792–800 (2013).
- Tian, D. S. & Niu, S. L. A global analysis of soil acidification caused by nitrogen addition. *Environ. Res. Lett.* **10**, 024019 (2015).
- Cai, M., Schwartz, J. S., Robinson, R. B., Moore, S. E. & Kulp, M. A. Long-term effects of acidic deposition on water quality in a high-elevation great smoky mountains national park watershed: Use of an ion input–output budget. *Water, Air, Soil Pollut.* **209**, 143–156 (2009).
- Likens, G. E., Driscoll, C. T. & Buso, D. C. Long-term effects of acid rain: Response and recovery of a forest ecosystem. *Science* **272**, 244–246 (1996).
- Kopittke, P. M. et al. Identification of the primary lesion of toxic aluminum in plant roots. *Plant Physiol.* **167**, 1402–1411 (2015).
- Kochian, L. V. Cellular mechanisms of aluminum toxicity and resistance in plants. *Annu. Rev. Plant Physiol. Plant Mol. Biol.* **46**, 237–260 (1995).
- Kochian, L. V., Pineros, M. A., Liu, J. & Magalhaes, J. V. Plant adaptation to acid soils: the molecular basis for crop aluminum resistance. *Annu. Rev. Plant Biol.* **66**, 571–598 (2015).
- Rengel, Z. Role of calcium in aluminium toxicity. *New Phytol.* **121**, 499–513 (1992).
- Huang, J. W., Shaff, J. E., Grunes, D. L. & Kochian, L. V. Aluminum effects on calcium fluxes at the root apex of aluminum-tolerant and aluminum-sensitive wheat cultivars. *Plant Physiol.* **98**, 230–237 (1992).
- Shortle, W. C. & Smith, K. T. Aluminum-induced calcium deficiency syndrome in declining red Spruce. *Science* **240**, 1017–1018 (1988).
- Jasechko, S. et al. Terrestrial water fluxes dominated by transpiration. *Nature* **496**, 347–350 (2013).
- Matimati, I., Verboom, G. A. & Cramer, M. D. Nitrogen regulation of transpiration controls mass-flow acquisition of nutrients. *J. Exp. Bot.* **65**, 159–168 (2014).
- Wang, L., Good, S. P. & Caylor, K. K. Global synthesis of vegetation control on evapotranspiration partitioning. *Geophys. Res. Lett.* **41**, 6753–6757 (2014).
- McLaughlin, S. B. & Wimmer, R. Calcium physiology and terrestrial ecosystem processes. *New Phytol.* **142**, 373–417 (1999).
- Cramer, M. D., Hoffmann, V. & Verboom, G. A. Nutrient availability moderates transpiration in *Ehrharta calycina*. *New Phytol.* **179**, 1048–1057 (2008).
- Hubbard, R. M., Ryan, M. G., Giardina, C. P. & Barnard, H. The effect of fertilization on sap flux and canopy conductance in a *Eucalyptus saligna* experimental forest. *Glob. Chang. Biol.* **10**, 427–436 (2004).
- Phillips, N., Bergh, J., Oren, R. & Linder, S. Effects of nutrition and soil water availability on water use in a Norway spruce stand. *Tree Physiol.* **21**, 851–860 (2001).
- Green, M. B. et al. Decreased water flowing from a forest amended with calcium silicate. *Proc. Natl. Acad. Sci. USA.* **110**, 5999–6003 (2013).
- Lanning, M. et al. Intensified vegetation water use under acid deposition. *Sci. Adv.* **5**, eaav5168 (2019).
- Lu, X. et al. Plant acclimation to long-term high nitrogen deposition in an N-rich tropical forest. *Proc. Natl. Acad. Sci. USA.* **115**, 5187–5192 (2018).
- Smith, K. T. & Shortle, W. C. Calcium amendment may increase hydraulic efficiency and forest evapotranspiration. *Proc. Natl. Acad. Sci. USA.* **110**, E3739 (2013).
- Wei, L., Ji, D., Miao, C., Muri, H. & Moore, J. C. Global streamflow and flood response to stratospheric aerosol geoengineering. *Atmos. Chem. Phys.* **18**, 16033–16050 (2018).
- Wu, J., Miao, C., Wang, Y., Duan, Q. & Zhang, X. Contribution analysis of the long-term changes in seasonal runoff on the Loess Plateau, China, using eight Budyko-based methods. *J. Hydrol.* **545**, 263–275 (2017).
- Frank, D. C. et al. Water-use efficiency and transpiration across European forests during the Anthropocene. *Nat. Clim. Chang.* **5**, 579–583 (2015).
- McDermid, S. S. et al. Disentangling the regional climate impacts of competing vegetation responses to elevated atmospheric CO₂. *J. Geophys. Res.: Atmos.* **126**, e2020JD034108 (2021).
- Wang, L. et al. Dryland productivity under a changing climate. *Nat. Clim. Chang.* **12**, 981–994 (2022).
- Singh, A., Kumar, S., Akula, S., Lawrence, D. M. & Lombardozzi, D. L. Plant growth nullifies the effect of increased water-use efficiency on streamflow under elevated CO₂ in the southeastern United States. *Geophys. Res. Lett.* **47**, e2019GL086940 (2020).
- Gedney, N. et al. Detection of a direct carbon dioxide effect in continental river runoff records. *Nature* **439**, 835–838 (2006).
- Cui, J. et al. Vegetation forcing modulates global land monsoon and water resources in a CO₂-enriched climate. *Nat. Commun.* **11**, 1–11 (2020).
- Zhu, Q. et al. Effects of future climate change, CO₂ enrichment, and vegetation structure variation on hydrological processes in China. *Glob. Planet. Change* **80–81**, 123–135 (2012).
- Kwon, H., Pendall, E., Ewers, B. E., Cleary, M. & Naithani, K. Spring drought regulates summer net ecosystem CO₂ exchange in a sagebrush-steppe ecosystem. *Agric. For. Meteorol.* **148**, 381–391 (2008).
- Ghimire, C. P. et al. Vapour pressure deficit and solar radiation are the major drivers of transpiration in montane tropical secondary forests in eastern Madagascar. *Agric. For. Meteorol.* **326**, 109159 (2022).
- Novick, K. A. et al. The increasing importance of atmospheric demand for ecosystem water and carbon fluxes. *Nat. Clim. Chang.* **6**, 1023–1027 (2016).
- Elvir, J. A., Wiersma, G. B., White, A. S. & Fernandez, I. J. Effects of chronic ammonium sulfate treatment on basal area increment in red spruce and sugar maple at the Bear Brook Watershed in Maine. *Can. J. For. Res.* **33**, 862–869 (2003).

37. Magill, A. H. et al. Long-Term Nitrogen Additions and Nitrogen Saturation in Two Temperate Forests. *Ecosystems* **3**, 238–253 (2000).
38. Nellemann, C. & Thomsen, M. G. Long-term changes in forest growth: potential effects of nitrogen deposition and acidification. *Water, Air, Soil Pollut.* **128**, 197–205 (2001).
39. Shortle, W. C., Smith, K. T., Minocha, R., Lawrence, G. B. & David, M. B. Acidic deposition, cation mobilization, and biochemical indicators of stress in healthy red spruce. *J. Environ. Qual.* **26**, 871–876 (1997).
40. Bukombe, B. et al. Soil geochemistry—and not topography—as a major driver of carbon allocation, stocks, and dynamics in forests and soils of African tropical montane ecosystems. *New Phytol.* **236**, 1676–1690 (2022).
41. Hu, Y. et al. Mycorrhizal fungi alleviate acidification-induced phosphorus limitation: evidence from a decade-long field experiment of simulated acid deposition in a tropical forest in south China. *Glob. Chang. Biol.* **28**, 3605–3619 (2022).
42. Cabon, A. et al. Cross-biome synthesis of source versus sink limits to tree growth. *Science* **376**, 758–761 (2022).
43. Gonzalez de Andres, E. et al. The role of nutritional impairment in carbon-water balance of silver fir drought-induced dieback. *Glob. Chang. Biol.* **28**, 4439–4458 (2022).
44. Xu, X., Yang, D., Yang, H. & Lei, H. Attribution analysis based on the Budyko hypothesis for detecting the dominant cause of runoff decline in Haihe basin. *J. Hydrol.* **510**, 530–540 (2014).
45. Li, Z. & Quiring, S. M. Identifying the Dominant Drivers of Hydrological Change in the Contiguous United States. *Water Resour. Res.* **57**, e2021WR029738 (2021).
46. Penuelas, J. et al. Increasing atmospheric CO₂ concentrations correlate with declining nutritional status of European forests. *Commun. Biol.* **3**, 1–11 (2020).
47. Bauters, M. et al. Increasing calcium scarcity along Afrotropical forest succession. *Nat. Ecol. Evol.* **6**, 1122–1131 (2022).
48. Liang, X. et al. Global response patterns of plant photosynthesis to nitrogen addition: a meta-analysis. *Glob. Chang. Biol.* **26**, 3585–3600 (2020).
49. Allan, R. P. et al. Advances in understanding large-scale responses of the water cycle to climate change. *Ann. N.Y. Acad. Sci.* **1472**, 49–75 (2020).
50. Kooperman, G. J. et al. Plant physiological responses to rising CO₂ modify simulated daily runoff intensity with implications for global-scale flood risk assessment. *Geophys. Res. Lett.* **45**, 12,457–412,466 (2018).
51. McCormick, E. L. et al. Widespread woody plant use of water stored in bedrock. *Nature* **597**, 225–229 (2021).
52. Hahm, W. J. et al. Bedrock vadose zone storage dynamics under extreme drought: consequences for plant water availability, recharge, and runoff. *Water Resour. Res.* **58**, e2021WR031781 (2022).
53. Druhan, J. L., Fernandez, N., Wang, J., Dietrich, W. E. & Rempe, D. Seasonal shifts in the solute ion ratios of vadose zone rock moisture from the Eel River Critical Zone Observatory. *Acta Geochim.* **36**, 385–388 (2017).
54. Schwinning, S. A critical question for the critical zone: how do plants use rock water? *Plant Soil* **454**, 49–56 (2020).
55. Wlostowski, A. N. et al. Signatures of Hydrologic Function Across the Critical Zone Observatory Network. *Water Resour. Res.* **57**, e2019WR026635 (2020).
56. Malcomb, J. D. et al. Assessing Temperate Forest Growth and Climate Sensitivity in Response to a Long-Term Whole-Watershed Acidification Experiment. *J. Geophys. Res. Biogeosci.* **125**, e2019JG005560 (2020).
57. Elliott, K. J. et al. Water yield following forest–grass–forest transitions. *Hydrol. Earth Syst. Sci.* **21**, 981–997 (2017).
58. Xiong, X., Zhou, G., Zhang, D. & Zhou, G. Soil organic carbon accumulation modes between pioneer and old-growth forest ecosystems. *J. Appl. Ecol.* **57**, 2419–2428 (2020).
59. He, J. et al. The first high-resolution meteorological forcing dataset for land process studies over China. *Sci. Data* **7**, 25 (2020).
60. Beck, H. E. et al. MSWEP V2 Global 3-Hourly 0.1° Precipitation: Methodology and Quantitative Assessment. *Bull. Amer. Meteorol. Soc.* **100**, 473–500 (2019).
61. Beck, H. E. et al. MSWEP: 3-hourly 0.25° global gridded precipitation (1979–2015) by merging gauge, satellite, and reanalysis data. *Hydrol. Earth Syst. Sci.* **21**, 589–615 (2017).
62. Funk, C. et al. The climate hazards infrared precipitation with stations—a new environmental record for monitoring extremes. *Sci. Data* **2**, 150066 (2015).
63. Wu, J. et al. Prolonged acid rain facilitates soil organic carbon accumulation in a mature forest in Southern China. *Sci. Total Environ.* **544**, 94–102 (2016).
64. Keyimu, M. et al. Spatial differences in the radial growth responses of black locust (*Robinia pseudoacacia* Linn.) to climate on the Loess Plateau, China. *Dendrochronologia* **67**, 125832 (2021).
65. Islam, M., Rahman, M. & Bräuning, A. Long-term wood anatomical time series of two ecologically contrasting tropical tree species reveal differential hydraulic adjustment to climatic stress. *Agric. For. Meteorol.* **265**, 412–423 (2019).
66. Core-Team, R. R.: A language and environment for statistical computing. In: R. C. Team (Ed.). R Foundation for Statistical Computing, Vienna, Austria. (2019).
67. Bunn, A. G. & Korpela, M. An Introduction to dplyr. The Comprehensive R Archive Network. (2018).
68. von Arx, G. & Carrer, M. Roxas – A new tool to build centuries-long tracheid-lumen chronologies in conifers. *Dendrochronologia* **32**, 290–293 (2014).
69. Lu, X. et al. Nitrogen deposition accelerates soil carbon sequestration in tropical forests. *Proc. Natl. Acad. Sci. USA.* **118**, e2020790118 (2021).
70. Liu, K. et al. Soil acidification in response to acid deposition in three subtropical forests of subtropical China. *Pedosphere* **20**, 399–408 (2010).
71. Liu, J., Zhou, G. & Zhang, D. Simulated effects of acidic solutions on element dynamics in monsoon evergreen broad-leaved forest at Dinghushan, China. Part 1: dynamics of K, Na, Ca, Mg and P. *Environ. Sci. Pollut. Res.* **14**, 123–129 (2007).
72. Zhou, G. et al. Quantifying the hydrological responses to climate change in an intact forested small watershed in Southern China. *Glob. Chang. Biol.* **17**, 3736–3746 (2011).
73. Roderick, M. L. & Farquhar, G. D. A simple framework for relating variations in runoff to variations in climatic conditions and catchment properties. *Water Resour. Res.* **47**, 1–11 (2011).
74. Li, Z. & Quiring, S. M. Investigating spatial heterogeneity of the controls of surface water balance in the contiguous United States by considering anthropogenic factors. *J. Hydrol.* **601**, 126621 (2021).
75. Cheng, S., An, X., Zhou, L., Tans, P. P. & Jacobson, A. Atmospheric CO₂ at Waliguan station in China: Transport climatology, temporal patterns and source-sink region representativeness. *Atmos. Environ.* **159**, 107–116 (2017).
76. Liu, L. et al. Background variations of atmospheric CO₂ and carbon-stable isotopes at Waliguan and Shangdianzi stations in China. *J. Geophys. Res.: Atmos.* **119**, 5602–5612 (2014).
77. Wang, N. Z., Li, M. & Li, B.-x. Characteristics of atmospheric CO₂ and CH₄ variation in the Waliguan area. *Sci. Technol. Vis.* **21**, 210–211 (2018).
78. Zhao, Y. C., Liu, P., Wang, J. Q. & Li, B. X. Global atmospheric monitoring results during 1991–2011 in Waliguan, China. *J. Qinghai Environ.* **24**, 32–35 (2014).
79. Wang, H. & Yu, X. Sensitivity analysis of climate on streamflow in north China. *Theor. Appl. Climatol.* **119**, 391–399 (2014).
80. Piao, S. et al. Evidence for a weakening relationship between interannual temperature variability and northern vegetation activity. *Nat. Commun.* **5**, 1–7 (2014).
81. Wang, T. et al. Emerging negative impact of warming on summer carbon uptake in northern ecosystems. *Nat. Commun.* **9**, 1–7 (2018).

Acknowledgements

This study was supported by the National Science Fund for Distinguished Young Scholars (No. 41825020) and Basic Research Program of Guangzhou Science and Technology Bureau (No. 2022000156). We are also grateful to the colleagues who conducted the field sample and measurements: Deqiang Zhang, Qianmei Zhang, Guowei Chu, Jun Jiang and Pingping Xu. Tree ring sampling and software ROXAS measurement were greatly supported by Jingshu Wei, Maierdang Keyimu and Zongshan Li (Research Center for Eco-Environmental Sciences-CAS).

Author contributions

L.H.W., L.X.W. and J.Y. conceived and designed the experiments; M.Y. and S.Y. performed the experiments; L.H.W., M.L. and L.T. analyzed the data; L.T. and H.Y. contributed materials/analysis tools; L.H.W., L.X.W. wrote the paper.

Competing interests

The authors declare no competing interests.

Additional information

Supplementary information The online version contains supplementary material available at <https://doi.org/10.1038/s43247-023-01029-4>.

Correspondence and requests for materials should be addressed to Junhua Yan.

Peer review information *Communications Earth & Environment* thanks Kevin Smith, Kara Webster and the other, anonymous, reviewer(s) for their contribution to the peer review of this work. Primary Handling Editor: Aliénor Lavergne. A peer review file is available.

Reprints and permission information is available at <http://www.nature.com/reprints>

Publisher's note Springer Nature remains neutral with regard to jurisdictional claims in published maps and institutional affiliations.



Open Access This article is licensed under a Creative Commons Attribution 4.0 International License, which permits use, sharing, adaptation, distribution and reproduction in any medium or format, as long as you give appropriate credit to the original author(s) and the source, provide a link to the Creative Commons licence, and indicate if changes were made. The images or other third party material in this article are included in the article's Creative Commons licence, unless indicated otherwise in a credit line to the material. If material is not included in the article's Creative Commons licence and your intended use is not permitted by statutory regulation or exceeds the permitted use, you will need to obtain permission directly from the copyright holder. To view a copy of this licence, visit <http://creativecommons.org/licenses/by/4.0/>.

© The Author(s) 2023